University of Groningen

# Revisiting the Mechanism of the Meso-to-α Transition of Isotactic Polypropylene and Ethylene-Propylene Random Copolymers

Di Sacco, Federico; Saidi, Sarah; Hermida-Merino, Daniel; Portale, Giuseppe

*Published in:*
Macromolecules

*DOI:*
10.1021/acs.macromol.1c01904

**IMPORTANT NOTE: You are advised to consult the publisher's version (publisher's PDF) if you wish to cite from it. Please check the document version below.**

*Document Version*
Publisher's PDF, also known as Version of record

*Publication date:*
2021

Link to publication in University of Groningen/UMCG research database

*Citation for published version (APA):*
Di Sacco, F., Saidi, S., Hermida-Merino, D., & Portale, G. (2021). Revisiting the Mechanism of the Meso-to-α Transition of Isotactic Polypropylene and Ethylene-Propylene Random Copolymers. *Macromolecules*, *54*(20), 9681–9691. https://doi.org/10.1021/acs.macromol.1c01904

**Copyright**
Other than for strictly personal use, it is not permitted to download or to forward/distribute the text or part of it without the consent of the author(s) and/or copyright holder(s), unless the work is under an open content license (like Creative Commons).

The publication may also be distributed here under the terms of Article 25fa of the Dutch Copyright Act, indicated by the "Taverne" license. More information can be found on the University of Groningen website: https://www.rug.nl/library/open-access/self-archiving-pure/taverne-amendment.

**Take-down policy**
If you believe that this document breaches copyright please contact us providing details, and we will remove access to the work immediately and investigate your claim.

*Downloaded from the University of Groningen/UMCG research database (Pure): http://www.rug.nl/research/portal. For technical reasons the number of authors shown on this cover page is limited to 10 maximum.*

Macromolecules

pubs.acs.org/Macromolecules

Article

# Revisiting the Mechanism of the Meso-to-α Transition of Isotactic Polypropylene and Ethylene–Propylene Random Copolymers

Federico Di Sacco, Sarah Saidi, Daniel Hermida-Merino,* and Giuseppe Portale*

Cite This: *Macromolecules* 2021, 54, 9681–9691

Read Online

ACCESS | Metrics & More | Article Recommendations | Supporting Information

**ABSTRACT:** In this work, we have conducted *in situ* simultaneous small- and wide-angle X-ray scattering and Raman spectroscopy experiments to investigate the fundamental differences in the mechanism of the mesomorphic to α phase transition of the isotactic polypropylene homopolymer and the random ethylene–propylene copolymer. *Via* quantitative analysis of the results coming from the three techniques, we found that in the homopolymer, chain interlock and chain extension occur during the transition. However, these processes are not necessary for the transition to occur. Indeed, the presence of randomly distributed ethylene co-units hinders the chain interlock process in the early stages of the phase transition ($T > 60$ °C) and suppresses the chain elongation process at the later stages ($T > 90$ °C). Consequently, the mesomorphic to α-phase transition in the random copolymer occurs with inclusion of the ethylene co-units inside the crystal lattice, causing increased lateral interchain distance and larger crystalline sizes. Our results show how differences exist in the way solid phase transitions occur at the molecular scale when co-monomers are included into the macromolecular chains, leading to a better understanding of the thermal behavior of semi-crystalline polymers.

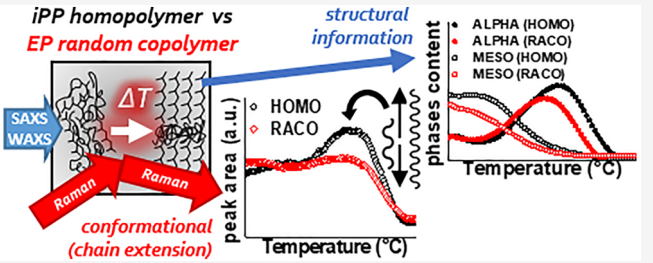


## 1. INTRODUCTION

Semi-crystalline polymers are characterized by great versatility in terms of both crystal structure and morphology.[1,2] The final properties of the materials can be tuned by adjusting the backbone composition and the crystallization conditions, allowing semi-crystalline polymers to be applied not only as daily commodities but as high-performance materials too. Isotactic polypropylene (iPP) is one of the most used semi-crystalline polymers worldwide, thanks to its easy processability and to the wide range of properties such as mechanical rigidity, thermal resistance, and chemical inertia. Particularly, optical and mechanical performances can be tailored by controlling the degree of isotacticity or by modifying the chain regularity *via* insertion of comonomers (ethylene and higher α-olefins), yielding regio-defects and stereo-defects. Moreover, the complex polymorphic behavior of iPP is of great interest, with five known crystal modification ranging from α to ε.[3,4] In addition, iPP features a solid metastable phase, the so-called mesomorphic phase or mesophase, characterized by an order degree significantly lower than that of the long-range ordered α monoclinic structure.

The mesophase is obtained by cooling the melt to low temperature at speed higher than 100 °C/s and thus, suppressing the formation of the α monoclinic structure.[5,6] The mesophase formation is inhibited when the melt is rapidly quenched at rates above 1000 °C/s to below the glass-transition temperature, yielding a fully amorphous solid. The use of intermediate cooling rates allows the coexistence of both mesomorphic and α monoclinic polymorphs. Within the mesophase crystals, the iPP chains are organized in bundles of 3/1 ordered helical chains along the chain axis direction, while significant disorder is present in the lateral direction where random packing of left- and right-handed helix produces a less densely packed crystal structure.[7−9] Morphologically, the mesophase presents nodular domains with size ranging from 5 to 20 nm that are characterized by the lack of the typical long-range order of spherulitic structures.[10] However, by heating to temperatures close to 70 °C, mesomorphic domains undergo a solid phase transition to the more stable α monoclinic structure. The meso-to-α phase transition occurs within the globular nodules, preserving the globular morphology with only a moderate increase in the domain size.[10−12] The meso-to-α phase transition ultimately affects the mechanical and optical properties of iPP, yielding ductile and transparent products that still possess high crystallinity.

An effective approach to modify the iPP properties is the tailored introduction of defects inside the crystalline structure that is often accomplished by modifying the stereo- and regio-

Received: September 8, 2021
Revised: September 28, 2021
Published: October 8, 2021

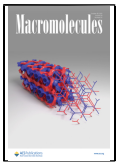

Downloaded via 82.174.118.135 on November 15, 2021 at 11:31:59 (UTC).
See https://pubs.acs.org/sharingguidelines for options on how to legitimately share published articles.

ACS Publications

© 2021 The Authors. Published by American Chemical Society



https://doi.org/10.1021/acs.macromol.1c01904
*Macromolecules* 2021, 54, 9681–9691

regularity of the chains[13,14] or by the addition of comonomers.[15] In comparison to homopolymeric grades, random copolymers of iPP are characterized by lower crystallinity, better optical transparency, along with a higher toughness that are defined by the nature and amount of the used comonomers. The presence of comonomeric defects hampers the crystallization process and slows the growth of the $\alpha$ phase spherulites by reducing the length of crystallizable sequences, regardless of the defect nature.[16] The mechanical[17] and optical properties[18,19] of the random copolymer can be tuned accordingly to meet the required application.

The crystallization and melting of iPP and their copolymers have been largely investigated using differential scanning calorimetry (DSC), optical and electron microscopy, atomic force microscopy, and small-/wide-angle X-ray scattering (SAXS/WAXS).[12,20−22] Recently, *in situ* synchrotron SAXS/WAXS has been successfully used to elucidate the crystallization behavior and structural domain formation at the nanoscale under several conditions (fast cooling/heating, uniaxial stretching, and applied flow).[23−25] However, changes occurring at the conformational level of the chains during thermal treatments or phase transitions are hardly detectable by X-ray scattering measurements. Likewise, spectroscopic tools, such as Fourier transform infrared (FTIR) or Raman spectroscopy, play an important role to probe macromolecular reorganization *via* monitoring the evolution of particular vibrational bands, in particular the so-called "regularity bands."[26] The regularity bands correspond to the helical chains composed by a fixed number of monomeric units in which identification and assignment have been extensively investigated in recent years.[27−29]

Herein, an *in situ* simultaneous SAXS/WAXS/Raman study was performed on an iPP homopolymer and on a random ethylene−propylene copolymer (RACO) to elucidate the precise correlation between changes occurring at the level of the chain conformation (by Raman spectroscopy and multivariate analysis), in the local packing of the chains (by WAXS), in the nanoscale organization of the chains (by SAXS), and to understand the effect of the comonomer inclusion on these conformational changes during the disorder-to-order solid transition. To the best of our knowledge, the effects of comonomer partition during the conformational chain reorganization with the meso-to-$\alpha$ transition have not been investigated in detail until now, despite being of utmost importance for both academia and plastic industry.

## 2. MATERIALS AND METHODS

Both polymers used in this study were provided by Borealis-GmbH (Linz, Austria). Namely, an iPP homopolymer called HOMO and a propylene−ethylene random copolymer with 2.2 wt % of C2 monomer called RACO. The two polymers have a very comparable polydispersity. An overview of the polymer characteristics is present in Table 1.

**Table 1. Overview of the Polymer Characteristics[a]**

| polymer name | $T_{melt}$ (°C) | isotacticity <mm> (%) | regio-defects | $M_w/M_n$ | C2 monomer (wt %) |
|---|---|---|---|---|---|
| HOMO | 154 | 99.2 | 0.7 | 3.5 | 0 |
| RACO | 152 | 96.5 | 0 | 3.4 | 2.2 |

[a]The melt flow rate (MFR) at 230 °C/2.16 kg is 8 g/10 min for both.

The materials were received as films of 50 $\mu$m thick, produced *via* cast film extrusion using a Collin machine. The Collin extruder used has a diameter of 30 mm and an $L/D$ ratio of 30, with a multi-purpose screw capable of a maximal throughput of 15 kg/h. The attached cast film die features a width of 300 mm and a die gap of 0.5−1 mm (set at 0.5 mm for a 50 $\mu$m film). The chill roll and secondary roll possess a width of 350 mm and a diameter of 144 mm, and both can be set to the temperature range of 15−150 °C. In this study, both polymers have been extruded to target the highest amount of the mesomorphic phase (chill roll cooled to a 15 °C). *In situ* simultaneous SAXS/WAXS coupled with Raman measurements (SAXS/WAXS/Raman) were performed at the beamline BM26B-DUBBLE at the ESRF[30,31] (Figure 1) using an X-ray wavelength of 0.1 nm and an X-ray spot size of 300

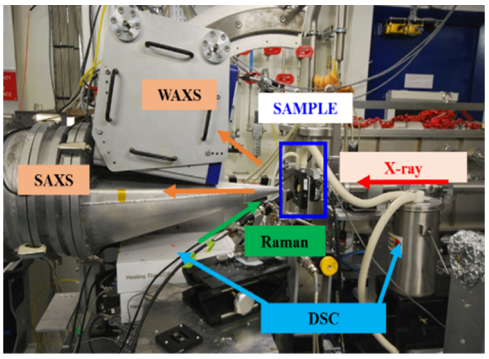


**Figure 1.** *In situ* SAXS/WAXS/Raman setup at ESRF (Grenoble, FR). A Linkam DSC stage is used to control the temperature profile.

$\mu$m × 400 $\mu$m on the sample. Prior to the measurements, the polymer films were encapsulated inside a standard DSC aluminum pan with a pierced lid equipped with a thin mica window to permit the accessibility of the Raman laser. The samples were heated from ambient temperature up to 200 °C at a heating rate of 5 °C/min using a Linkam DSC600 heating−cooling stage system.

A metal spring has been used to ensure a stable position and an adequate contact with the heating plate of the Linkam DSC device placed vertically during the acquisition process. SAXS and WAXS patterns were collected using a PILATUS 1M and a PILATUS 300K-W detector, respectively, with an acquisition time of 30 s. The detectors were positioned, respectively, at 5000 and 280 mm away from the sample for SAXS and WAXS analyses, respectively. The WAXS patterns were collected in the $q$-space region from 6 to 20 $nm^{-1}$, while the SAXS patterns were recorded in the $q$-space region from 0.1 to 1 $nm^{-1}$. A background pattern was acquired using an empty cell, and it was subtracted from the sample patterns before the reduction of the acquired data to 1D profiles using the python-based Bubble program[32] available at the beamline. The $q$-scale was calibrated using the known peak position from a standard silver behenate sample for SAXS and from a standard $Al_2O_3$ powder for WAXS. Both standards were purchased from NIST.

To account for changes in the structural and phase composition of each sample during the meso-to-$\alpha$ transition, WAXS patterns were fitted using a multi-peak fitting routine, with Voigt functions for the deconvolution of each scattering reflection. According to eq 1, the crystallinity of each phase is calculated as

$$X_i(T) = \frac{A_i(T)}{A_{tot}(T)} \quad (1)$$

where $X_i$ is the fraction of the selected phase at temperature $T$, $A_i$ is the overall integrated area of the selected crystalline phase reflections, and $A_{tot}$ corresponds to the total integrated area of the WAXS pattern. Figure S1 shows an example of a deconvoluted pattern for a sample at a temperature where the $\alpha$ phase dominates. Hereby, the evolution over time of each crystalline phase was monitored from ambient temperature up to above the melting transition.


https://doi.org/10.1021/acs.macromol.1c01904
Macromolecules 2021, 54, 9681−9691

Long period (Lp) and average domain size (lc) evolution with temperature were calculated, according to the so-called linear electron density correlation function, using eq 2[33]

$$\gamma(r) = \int_0^\infty q^2 I(q)\cos(qr)\mathrm{d}q \quad (2)$$

where $I(q)$ is the scattering intensity and $r$ is the distance in real space. Lp was calculated from the maximum of the first oscillation above zero of the $\gamma(r)$, while lc was calculated using the so-called correlation triangle method.[34] Figure 2 shows a collection of different correlation

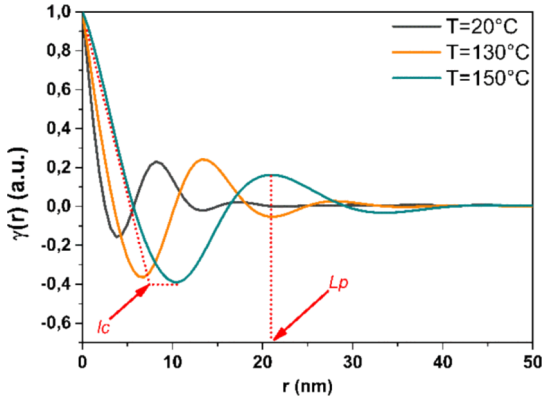


**Figure 2.** Example of linear electron density correlation function for sample HOMO, calculated at three different temperatures: 20 °C (gray), 130 °C (orange), and 150 °C (cyan). Increase in the domain size is appreciable by the shift of the first maximum toward a higher value of $r$.

functions taken at three different temperatures for the HOMO grade. The value of long period (Lp) is retrieved from the position of the first maximum. The average domain size (lc) is calculated by the intersection between the slope of the linear part of the curve at $r$ value close to zero, obtained by simple linear regression, and the tangent to the curve at the absolute minimum. This intersection defines the sides of the so-called correlation triangle. Both the long period and the average domain size increase with the temperature during heating. The curve maximum at the highest shown temperature (150 °C) exhibits a drop in intensity as a result of the partial melting of the sample, indicating the loosening of structural correlation when going from an ordered to a partially molten structure.

Raman measurements were performed simultaneously to SAXS/WAXS using an RXN-1 spectrometer by Kaiser Optical equipped with a fiber optics with a focal distance of 50 mm and a wavelength of 785 nm. Spectra were acquired every 10 s, with a delay of 5 s between each acquisition. The acquisition range was set between 350 and 1700 $cm^{-1}$. The Raman measurements were recorded in the total darkness to ensure the absence of light artefacts. Moreover, a background spectrum was registered using an empty aluminum pan/lid system. All spectra were normalized to the intensity of the band at 1456 $cm^{-1}$ (deformation vibration of $CH_3$ groups), which is not influenced by the degree of crystallinity and by the degree of conformational order of the polymer chains,[35] and subsequently, the band area was integrated using a fitting routine. The area of each diagnostic band was evaluated after baseline subtraction to determine the conformational changes during the meso-to-$\alpha$ transition. Both for X-rays and Raman, data analysis was conducted using the MATLAB software, and plots were generated using the Origin software.

## 3. RESULTS OVERVIEW

Figure 3 shows the overview of the evolution of the simultaneously acquired WAXS, SAXS, and Raman profiles allowing us to obtain information on the structural, morphological, and conformational evolution during heating.

The development of the WAXS intensity profiles for both the homopolymer iPP (HOMO) and the RACO is illustrated in Figure 3a,b. Initially, both polymers featured the mesomorphic phase characterized by the two typical broad scattering reflections centered at 10.61 and 15.12 $nm^{-1}$.[36,37] The formation of the mesomorphic phase is consistent with the high cooling rate to which both materials were subjected during production as a consequence of the low chill roll temperature of 15 °C used to process the sample.[38]

At temperatures >50 °C, the two mesomorphic reflections gradually disappeared and were replaced by the (110), (040), (130), and (131) characteristic reflections of the $\alpha$ monoclinic phase. It is found that the onset of the meso-to-$\alpha$ phase transition occurs earlier for the RACO sample than that for the HOMO sample, as a consequence of the lower thermal stability of the RACO mesomorphic structure.[9,39] The onset of the meso-to-$\alpha$ phase transition, as observed by WAXS, is approximately 60 and 70 °C for the RACO and HOMO iPP grades, respectively. Full conversion of the mesomorphic phase to the $\alpha$-monoclinic phase is achieved at around 120 °C. Heating at temperature higher than the melting point for both grades (~155 °C) ensures complete disappearance of any WAXS reflection associated with the presence of crystalline order and thus complete melting of the polymers.

The evolution of the sample crystallinity (sum of the mesophase and the crystalline $\alpha$-phase content), as extracted from analysis of the WAXS profiles, is reported in Figure S2. Generally, the HOMO grade develops an overall higher degree of crystallinity if compared to the RACO, which is in line with the expected higher perfection of the homopolymer molecular architecture. The initial drop in total crystallinity at low temperature ($T$ < 60 °C) is associated with an apparent increase in the amorphous scattering halo that will be discussed later. The nanostructure evolution associated with the meso-to-$\alpha$ transition was additionally monitored by simultaneous SAXS measurements. Figure 3c,d shows the evolution of the Lorentz corrected SAXS intensity profiles with temperature for the HOMO and RACO grades, respectively. A weak scattering peak close to 0.7 $nm^{-1}$ is present at room temperature in both polymers. This is consistent with the low degree of long-range order and the weak spatial correlation of the globular mesophase domains dispersed within the amorphous matrix.[40,41] The transition toward the more ordered $\alpha$-monoclinic crystals is clearly visible by monitoring both the intensity increases and the peak shift taking place during heating, associated, respectively, to an increase in the number of ordered crystalline segments and to a growth in the average crystalline domain sizes and spacing. Upon heating, the peak position shifts from about 0.7 $nm^{-1}$ to about 0.4 $nm^{-1}$. The SAXS observations agree with the improvement in the crystal arrangement observed by WAXS. Upon melting, the SAXS intensity drops sharply until disappearing completely, indicating loss of any structural order inside the molten material.

The temperature evolution of some representative Raman spectra in the spectral range from 400 to 1600 $cm^{-1}$ for the HOMO and RACO is reported in Figure 3e,f, respectively. For the sake of image clarity, we selected only a few of the numerous recorded spectra, starting from room temperature up to the full melt condition (20−200 °C), with an increment of 20 °C between each profile. At temperature below the melting point, well-defined peaks associated with different vibrational modes are recognizable. The diagnostic regularity bands at 973 $cm^{-1}$ (CH bending, C−C stretching), 998 $cm^{-1}$


https://doi.org/10.1021/acs.macromol.1c01904
Macromolecules 2021, 54, 9681−9691

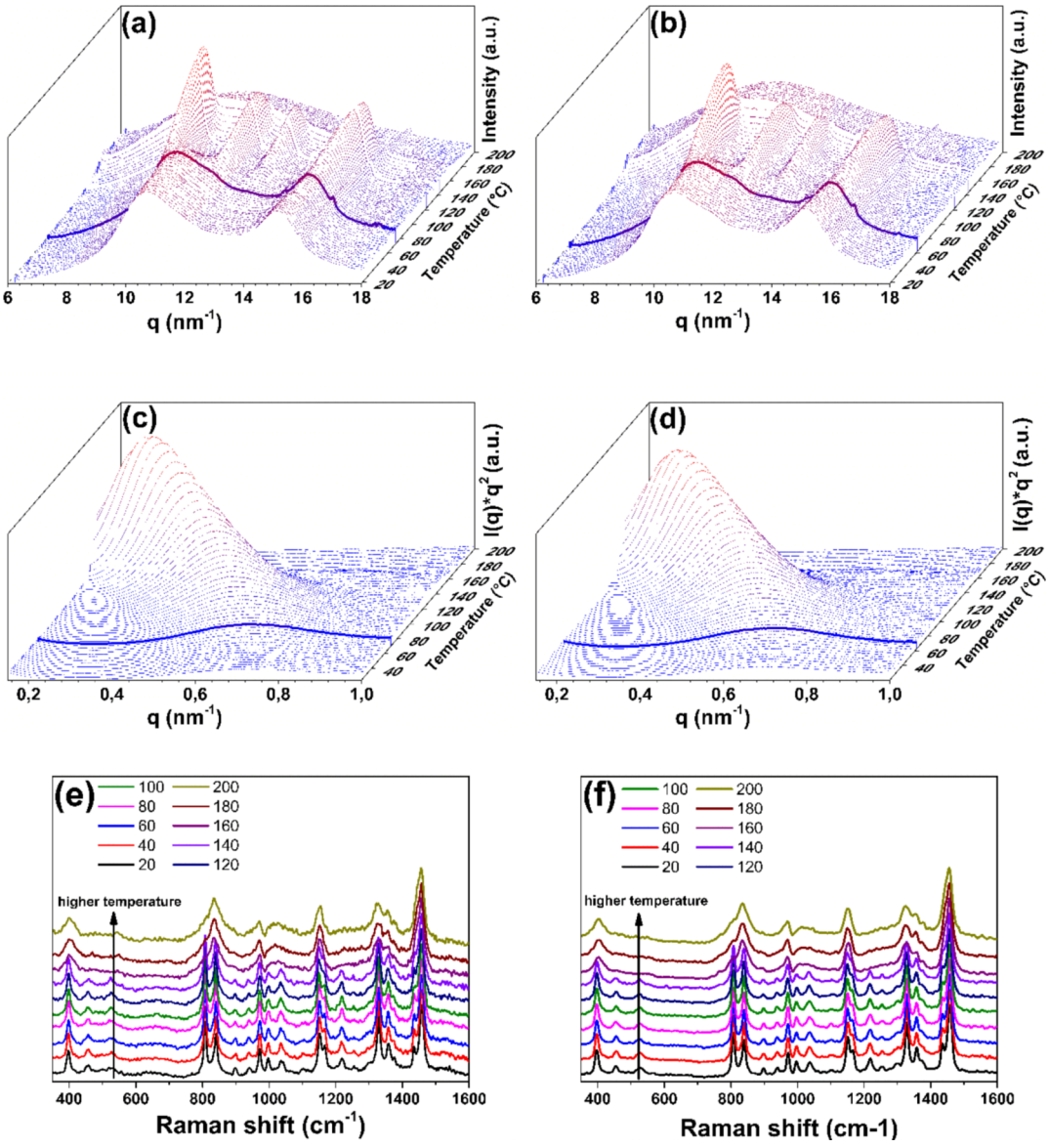


**Figure 3.** (a–f): Summary of the results simultaneously obtained during the *in situ* analysis of (left panels) an iPP homopolymer (HOMO) and (right panels) a random poly(ethylene propylene) copolymer (RACO). (a,b) WAXS intensity profiles as a function of temperature for HOMO and RACO, respectively; the thicker profiles denote the onset of the meso-to-$\alpha$ phase transition (c,d) Lorentz corrected SAXS $I(q)q^2$ profiles as a function of temperature for HOMO and RACO, respectively; (e,f) selected Raman spectra as a function of temperature for HOMO and RACO, respectively. The Raman spectra have been shifted vertically for clarity.

($CH_3$ rocking, CH bending), 841 $cm^{-1}$ ($CH_2$ rocking, C–$CH_3$ stretching), and 1220 $cm^{-1}$ ($CH_2$ twisting, C–$CH_3$ stretching, CH bending) can be assigned to helical chain segments composed by 5, 10, 12, and 14 monomeric units, respectively. Two additional bands can be identified at 400 $cm^{-1}$ (C–C–C bending and CH bending) and 1300 $cm^{-1}$ (CH bending and $CH_2$ twisting) that are not classified as regularity bands. Their vibrational modes can be used to describe the conformational order along the parallel (400 $cm^{-1}$) and perpendicular (1300 $cm^{-1}$) directions with respect to the helical chain axis (*e.g.*,: the polypropylene *c*-axis). Another band at 809 $cm^{-1}$ ($CH_2$ rocking, C–$CH_3$ stretching, and C–C stretching) is clearly detected, and it is often used to determine the overall crystallinity in iPP samples.[26,42] The vibrational bands lying at frequencies higher than 1400 $cm^{-1}$ are not associated to the vibrational coupling of atoms within chains and crystals, and thus, are not considered as regularity bands.[20,26,27] It is clear that conformational rearrangements take place for both grades during the meso-to-$\alpha$ transition and the melting transition. Generally, for both grades, the intensity of all the bands drops abruptly as the melting temperature is approached. The persistency of some of the bands (400, 973, 998, and 1300 $cm^{-1}$) after melting is consistent with the preservation of a certain degree of conformational order in iPP after transition to the melting state.[43]

Besides tracing the thermal transitions, the simultaneous acquisition of SAXS, WAXS, and Raman data allows us to perform a quantitative description of the structural and conformational changes occurring during the transitions and enables us to elucidate the influence of the presence of the ethylene co-units on the meso-to-$\alpha$ phase transition, which we discuss in the next section.



https://doi.org/10.1021/acs.macromol.1c01904
*Macromolecules* 2021, 54, 9681–9691

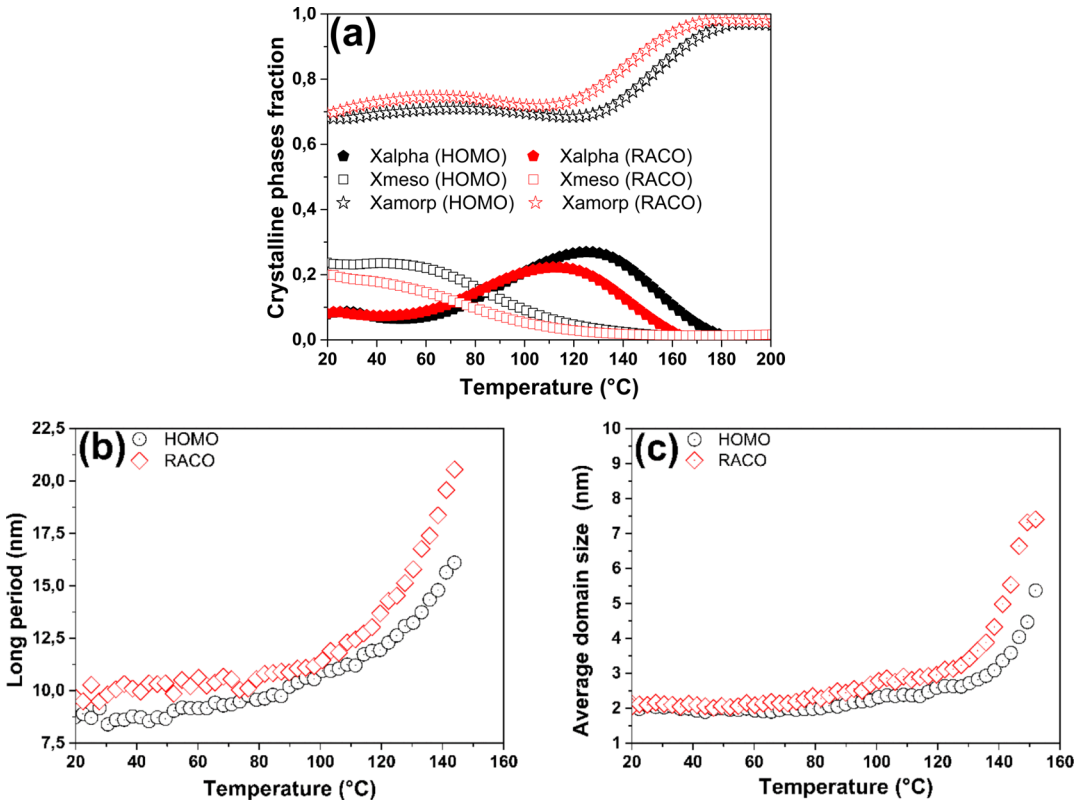


**Figure 4.** (a–c) (a) Evolution of crystalline phases for both grades as a function of temperature (HOMO-full points, RACO-hollow points); (b,c) evolution of long period and average domain size, calculated from 1DCF, as a function of temperature, for both grades.

## 4. QUANTITATIVE ANALYSIS AND DISCUSSION

The phase content evolution during heating, as obtained from the WAXS intensity deconvolution, is reported in Figure 4a. At room temperature, the initial mesophase content is about 24% for the HOMO and 20% for the RACO. The slightly higher mesophase content of the HOMO is related to the mechanism of molecular arrangement, in which small, disordered, bundles of 3/1 helix chain attain a critical length value during the rapid temperature quench from the melt. The presence of chain defects in the RACO shortens the bundle length, further hindering the formation of the mesophase.[15] On heating, the complete conversion of the mesophase to the more ordered $\alpha$-monoclinic phase occurs, as widely reported in the literature.[45] The onset of the meso-to-$\alpha$ phase transition is recorded slightly earlier for the RACO sample (~50 °C) than that for the HOMO sample (~60 °C). Interestingly, the structural transformation for the RACO sample is not as well-defined as for the HOMO, and structural changes occur immediately upon heating from room temperature with a gradual decrease in the mesophase being readily observed (see Figure 4a).

We attributed the lower thermal stability of the RACO mesophase to its less stable nature due to the ethylene comonomer hindrance effect on the disordered chain packing. Moreover, the impact of the ethylene comonomers is equally reflected by a smaller value of the maximum $\alpha$-phase content attained by the RACO sample upon heating just before the melting process settled in (~20% for RACO against ~30% for HOMO). Thus, the presence of the ethylene comonomers has a negative impact both on the mesophase and $\alpha$-phase formation, in line with what reported previously in the literature.[16] Furthermore, a shift in the melting onset of the generated $\alpha$-phase is observed, occurring at 115 °C for the RACO and 130 °C for the HOMO iPP, reflecting the lower thermal stability of the less ordered RACO $\alpha$-phase crystalline domains.

Analysis of the amorphous fraction evolution shows an apparent increase in the amorphous phases occurring at temperature below the meso-to-$\alpha$ phase transition. This might be caused by changes in the polymer thermal expansion coefficient, which is known to be larger for the amorphous phase compare to crystalline phases[40] that influence the overall scattering intensity recorded during heating, resulting in an apparent growth of the amorphous fraction at low temperature. It is important to underline that cold-crystallization phenomena are very limited in our experiments. This is expected when using a constant heating rate (5 °C/s) which does not allow for sufficient time for a reorganization of the amorphous phase into a crystalline one during heating. Eventually, a sharp rise in the amorphous fraction is observed for $T$ > 140 °C for both grades because of the melting of the $\alpha$ monoclinic crystals.

To study the morphological transitions occurring at the nanoscale during heating, the long period and the average domain size were calculated from SAXS data *via* correlation function analysis (eq 2) and plotted against temperature in Figure 4b,c, respectively. It is worth to highlight that at temperature lower than that at the meso-to-$\alpha$ transition, the calculated values refer to the average dimension of the ordered and semi-ordered domains that represent the mesomorphic bundles which dominate the polymer structure at the beginning. Above the meso-to-$\alpha$ transition, the average domain size corresponds to the average dimension of the $\alpha$ crystallites. Interestingly, a larger long period for the RACO sample was measured across the entire temperature range under study. This can be explained by considering the lower rate of


https://doi.org/10.1021/acs.macromol.1c01904
Macromolecules 2021, 54, 9681–9691

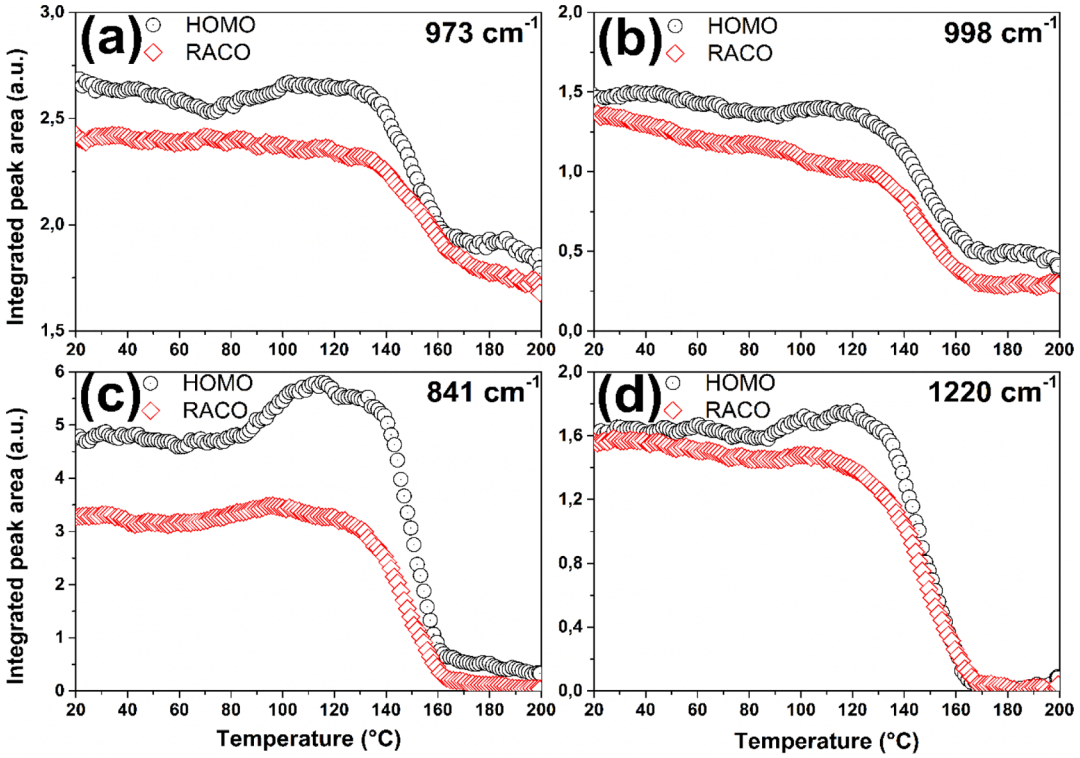


**Figure 5.** (a–d): Comparison between the area of the four regularity bands for both grades (HOMO—black plots; RACO—red plots) as a function of temperature. (a) Bands 973 $cm^{-1}$ (helical chain segments of 5 monomeric units); (b) bands 998 $cm^{-1}$ (helical chain segments of 10 monomeric units); (c) bands 841 $cm^{-1}$ (helical chain segments of 12 monomeric units); and (d) bands 1220 $cm^{-1}$ (helical chain segments of 14 monomeric units).

mesomorphic phase formation of the RACO compared to the similar homopolymeric grades[46] which cause an overall higher long period induced by the higher content of the amorphous fraction. This observation agrees with the WAXS deconvolution results for the RACO sample, showing a consistently higher amorphous fraction and a lower mesomorphic fraction with respect to the HOMO grade as a result of the slower crystallization rate in the random copolymer sample. An identical long period development during the heating cycle was probed for both samples up to the meso-to-$\alpha$ transition point. However, above the meso-to-$\alpha$ transition point, the trend in the long period *versus* temperature between the two polymers started to diverge, with a faster change of long period recorded for the HOMO iPP in the temperature range from 60 to 120 °C. This observation can be explained considering that the chain slipping process, and the following chain extension, occurring within the mesomorphic nodules[33] is hindered by the presence of the ethylene comonomers within the RACO sample during heating until 110 °C and consistent with the lower total crystallinity recorded for RACO by WAXS analysis. The influence of the comonomer presence on the chain slipping will be discussed in detail below using the Raman data. After reaching a temperature of 130 °C, the long period for both samples keeps increasing at a steeper rate which is connected with the start of the crystalline domain thickening process of the newly formed $\alpha$-monoclinic crystalline domains.[33,40] The complete loss of long-range correlation occurs at temperature nearby the melting point.

The evolution of the average domain size upon heating reveals also interesting differences between the two grades (Figure 4c). Up to the meso-to-$\alpha$ transition point, the average domain size is equal and constant with temperature for both samples. As already reported in the previous literature,[9,46] ethylene comonomers are included in the semi-ordered mesomorphic bundles with no change in the volume of the structural unit. On the other hand, for temperature higher than the meso-to-$\alpha$ transition, the increase in the average domain size for the random copolymer is constantly higher compared to the homopolymer. This might arise from inclusion of the ethylene co-units into the paracrystalline lattice of the newly formed $\alpha$-monoclinic crystals, even if the degree of inclusion is low if compared to higher $\alpha$-olefin comonomers such as 1-butene and 1-hexane.[47] Above the meso-to-$\alpha$ transition temperature, the thickening of the crystalline domains is observed for both polymers until melting temperature is reached.

While WAXS and SAXS are great tools to identify the structural changes occurring during the meso-to-$\alpha$ phase transition, they are neither capable to capture the changes occurring at the macromolecular chain level nor are they able to underline the possible differences that arise due to the chemical nature of the two PP samples. Here, a clear picture of the conformational changes associated with the meso-to-$\alpha$ phase transition is provided by our simultaneously acquired Raman spectroscopy data.

Figure 5a–d summarizes the trends in the peak intensity evolution upon heating for the four regularity bands that are associated to the presence of helical chain segments of variable lengths.[29,35,44] The evolution of the 5 and 10 unit bands is similar for both HOMO and RACO (Figure 5a,b). The band associated to the shorter helical segments of 5 units is practically constant until crystallite melting sets in, in agreement with the crystalline fraction evolution, as extracted


https://doi.org/10.1021/acs.macromol.1c01904
Macromolecules 2021, 54, 9681−9691

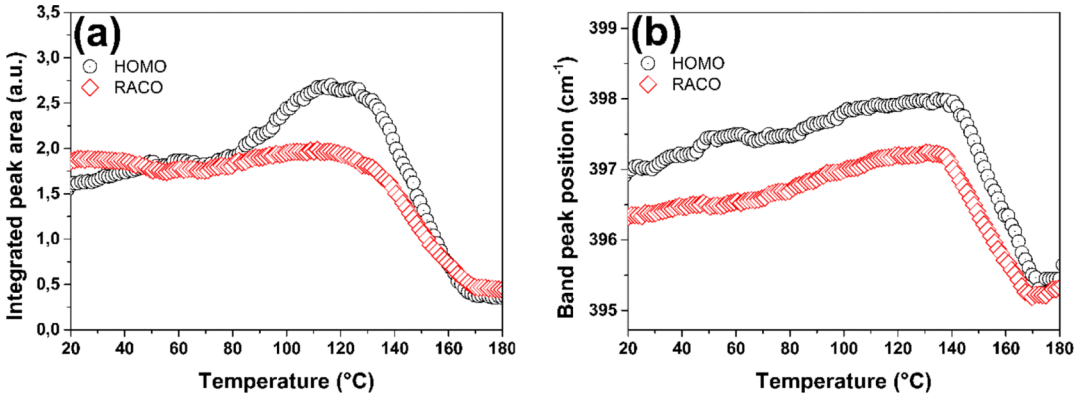


**Figure 6.** (a,b) (a) Area of band 400 cm$^{-1}$ evolution *vs* temperature for both grades and (b) peak position of band 400 cm$^{-1}$ shifting as a function of temperature.

by WAXS, confirming the extremely limited cold crystallization occurring in our samples.

Conversely, the 10 unit band is decreasing already before melting, suggesting chain rearrangement of these short-chain segments occurring inside the constricted mesomorphic domains. It is worth noticing that these two bands persist in the molten state, as already reported in the literature.[33] The most interesting observations are associated with the evolution of the bands related to helical segments with 12 and 14 units (Figure 5c,d). The 12 unit bands exhibit an intensity increase above the meso-to-$\alpha$ transition (~80 °C for the HOMO and ~60 °C for the RACO). Evolution of this band is associated with the onset of crystallization as Raman investigation on melt-crystallization experiments[29] showed that crystalline reordering begins when polymer chains form segments composed by this critical number of monomeric units. We reasonably expect that this critical length is maintained throughout a cold-crystallization process.

While the increase in intensity is marked for the HOMO polymer, it is more limited for the RACO polymer. For the 14 unit band, the intensity increase is observed only for the HOMO polymer.

The limited increase in the 14 unit band observed for the HOMO could be the result of an hampering effect of the crystallization occurring mostly inside the small, globular meso domains.[48] Indeed, previous studies highlighted that during isothermal crystallization, the 14 unit band appears and develops only after a rather long induction time.[28,49] For the RACO sample, the combined effect of both the small globular mesomorphic domains and the presence of the ethylene defects contribute toward hindering the formation of these longer helical chain segments.

The fundamental differences in the chain reorganization behavior observed here for the HOMO and RACO polymers can be discussed within the framework of a recent model proposed for iPP on the basis of FTIR studies.[33] Interchain conformation reorganization divided into a double-helix interlock process followed by chain slipping of adjacent folded-chain segments and the single-chain cluster aggregation was proposed to occur during the transition of the mesomorphic bundles to the $\alpha$ crystallites.[33] At first, two connected chain segments come close to each other to form an interlocked aggregate with opposite chain handedness. The conformational defects of the mesomorphic bundle begin to be adjusted by elongation of the stem and by chain rotation; both constituting the chain slipping process. Eventually, the reduction of the chains defects permits the two stems to come closer, increasing their package density and forming a compact aggregate. Then, the interlocked double-helix aggregates that are perfected by the chain slipping phenomena tend to coalesce with other clusters to form the crystal structure. This cascade of phenomena are considered to be strictly necessary to induce the transition from the disordered mesomorphic bundles to the more ordered crystalline $\alpha$ phase.[33] It is thus clear that the limited (or absent) increase of the 12 and 14 unit bands in the RACO polymer observed here suggests that chain elongation is not an active mechanism when ethylene comonomers are introduced in the iPP chains.

To further verify this hypothesis, we have studied also the behavior of the 400 cm$^{-1}$ band, assigned to the bending movements along the polymer backbone (C−C−C),[29] since chain extension is coupled with the enhancement of the vibrational modes occurring in the direction parallel to the polymer chain axis. Tracking of the band area evolution gives information on the total number of coupled oscillators referring to that mode, meaning that the evolution of the 400 cm$^{-1}$ band area can be used to study phenomena undergoing along the direction of the polymeric chains. On the other hand, shifts in the peak position can be used to recognize general changes in the conformational order which translate to an increase, or decrease, of the natural frequency of the oscillator.[29] The evolution of the area and peak position for the 400 cm$^{-1}$ band *versus* temperature is shown in Figure 6a,b for both polymers. A strong increase in band area at the onset of the meso-to-$\alpha$ transition is evident in the HOMO grade, meaning that the vibrational oscillators referring to the direction parallel to the chain axis increase in numbers and intensity, compatible with the chain extension phenomenon. In contrast, the RACO polymer displays an almost constant trend of the 400 cm$^{-1}$ band area, until melting occurs. It seems thus obvious that chain elongation phenomena are not significantly contributing to the transition of the random copolymer mesomorphic domains toward the $\alpha$-monoclinic crystals. Interestingly, a shift toward higher wavenumber is appreciable for both grades (Figure 6b), starting from the very beginning of the heating.

This blue-shift can be attributed to a continuous increase in the conformational disorder of the polymeric chains upon heating. This demonstrate that clear conformational changes occur in both polymeric grades but following different paths near the meso-to-$\alpha$ monoclinic transition, with the random copolymer not being able to perform a detectable chain


https://doi.org/10.1021/acs.macromol.1c01904
Macromolecules 2021, 54, 9681−9691

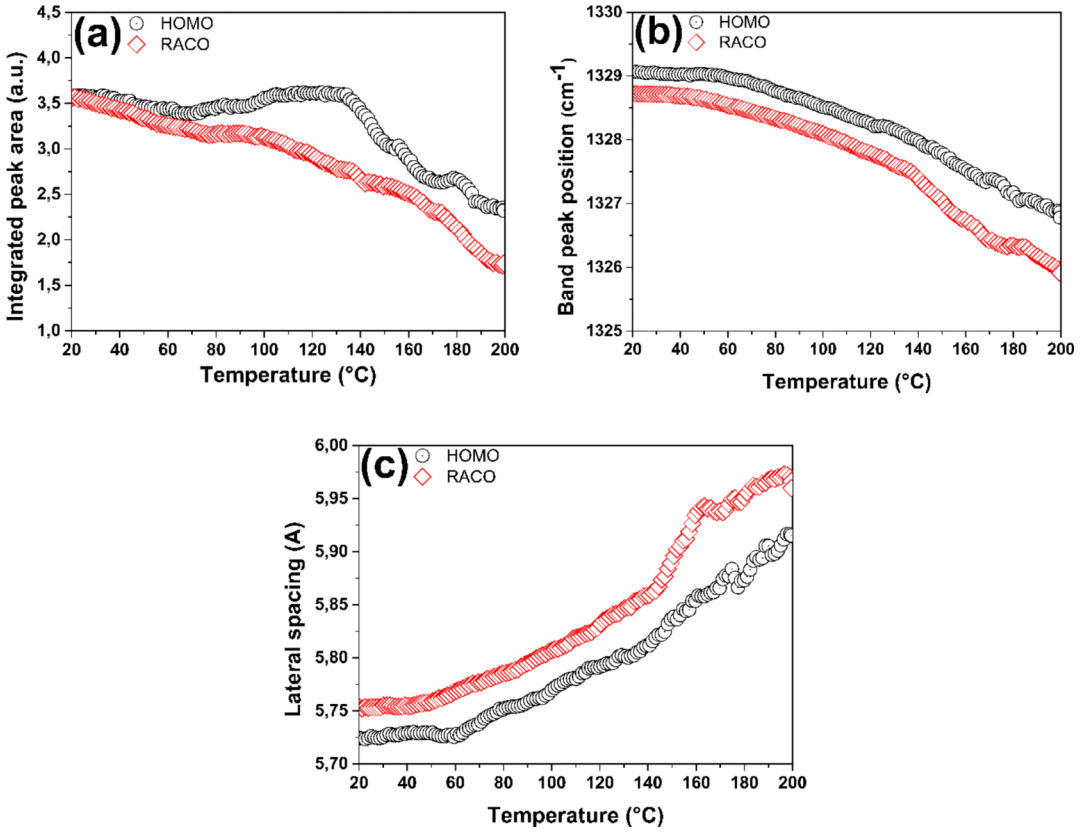


**Figure 7.** (a–c) (a) Area of band 1330 $cm^{-1}$ evolution *vs* temperature for both grades; (b) peak position of the band 1330 $cm^{-1}$ shifting as a function of temperature; and (c) trend of adjacent chain lateral spacing retrieved from peak position analysis of band 1330 $cm^{-1}$.

elongation throughout the process. This can be the result of the hindering effect of the ethylene co-units that produce a shortening of the repeating length of the newly formed $\alpha$ crystalline chains.

This phenomenon was speculated few years ago[16,50] and revised more recently by Li *et al.*,[33] suggesting that conformational reorganization following the sequence of *interlocking-to-chain elongation* could be hindered or suppressed *via* addition of co-monomers inside the molecular architecture of iPP material. However, on the contrary of what stated by the authors, our results demonstrate that translation from the disordered mesomorphic bundles toward the highly ordered $\alpha$-phase can occur also without significant elongation of the shorter ordered chain segments.

If chain elongation is effectively suppressed by ethylene units located along the polymer backbone, it is reasonable to speculate that the preceding chain interlocking process may also be influenced by the comonomer presence. Changes occurring along the direction perpendicular to the polymer chain axis (*e.g.*, adjacent interchain distance) can be assessed by following the evolution of the area and position of the band initially located around 1330 $cm^{-1}$ which is assigned to the twisting mode of $CH_2$ units (Figure 7a,b).

The position of the 1330 $cm^{-1}$ band is constant up to ~40–50 °C for the RACO and up to ~60 °C for the HOMO. After that, the band exhibits a marked red-shift as a result of promotion of $CH_2$ twisting motions and thermal expansion of the unit cell (Figure 7b). The earlier onset of the red-shift for the RACO polymer is in agreement with the lower thermal stability of its mesomorphic domains, also in agreement with WAXS observations. The peak shift of the 1330 $cm^{-1}$ band can be used to estimate the average lateral interchain spacing (see Figure 7c).[29] The increase in the lateral interchain distance is identical and linear up to the melting onset for the two polymers. However, a larger lateral spacing is estimated for the RACO polymer, having a spacing of 5.75 Å against the 5.72 Å of the HOMO sample. As expected for highly mesomorphic iPP grades, both spacings are attested to a lower value than the typical 5.9 Å for a slow-cooled, unconstrained lattice.[51]

Despite this similar thermal response in the lateral unit cell expansion, a fundamental difference between the two grades is observed when looking at the evolution of the band area upon approaching the respective meso-to-$\alpha$ transitions. Figure 7a shows an increase in the 1330 $cm^{-1}$ band intensity of the HOMO polymer for temperature higher than ~60 °C, while the band monotonically decreases upon heating for the RACO polymer. We associated the increase of the 1330 $cm^{-1}$ band area observed for the HOMO polymer to chain interlock and ejection of structural and conformational defects *via* chain rotation and slipping when approaching and crossing the meso-to-$\alpha$ transition. Indeed, interlock of adjacent helices with opposite handedness at temperatures above 50 °C was reported for the iPP homopolymer.[33] The presence of ethylene units in the RACO polymer seems to hinder this efficient interlocking and the subsequent chain perfection processes occurring in the direction perpendicular to the chain axis, even if a looser interlocking between defective adjacent chains can still occur without resulting in a significant increasing trend of the intensity of the 1330 $cm^{-1}$ band.

Additional evidence of the impact of ethylene co-units on the mechanism of evolution toward the $\alpha$-monoclinic form can be found by quantitative analysis of the evolution of the two


https://doi.org/10.1021/acs.macromol.1c01904
Macromolecules 2021, 54, 9681–9691

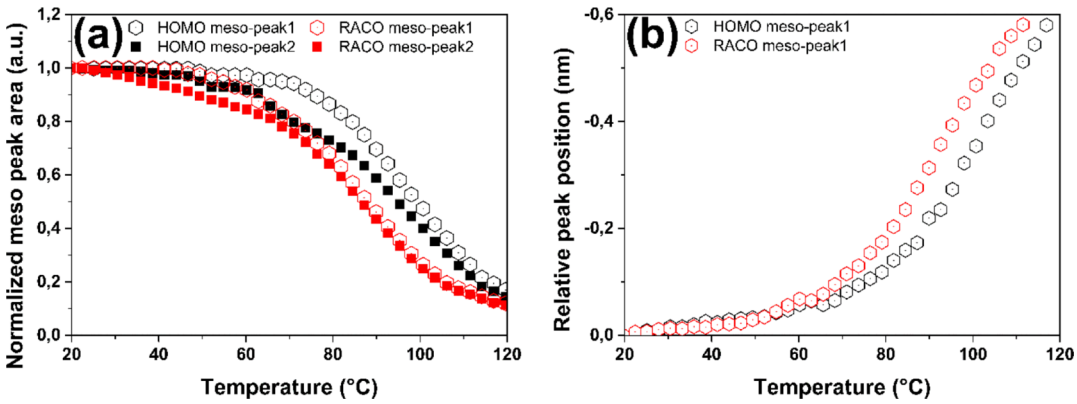


**Figure 8.** (a,b) (a) Normalized peak area of mesophase scattering reflection for both grades as a function of temperature and (b) relative shift of the mesophase peak position with respect to the initial value as a function of temperature for both grades.

main mesophase WAXS reflections. Figure 8a,b reports the behavior of the area and position of the two main mesomorphic WAXS reflections *versus* temperature for the two investigated grades.

The shift in the position of the mesomorphic scattering reflection located at lower $q$-values ($q$ = 10.61 $nm^{-1}$ named here meso-peak1) is attributed to changes in the interchain correlation,[9] while the reflection at higher $q$-values ($q$ = 15.12 $nm^{-1}$ named here meso-peak2) refers to the repeating period (pitch) along the helices.[6] The normalized area intensity shows differences in the overall stability for the two mesophases. Upon heating, the meso-peak1 remains stable up to ∼60 and ∼40−50 °C for the HOMO and RACO polymers, respectively. From that point on, the trends start to diverge, with the RACO grades showing a steeper decrease in intensity. This agrees with the already discussed lower stability of the RACO mesophase which transforms at lower temperature if compared to the less defective HOMO mesophase, and it is also in agreement with the onset of the lateral interchain distance expansion observed by Raman spectroscopy. A more interesting difference is observed in the evolution of the meso-peak2, which is associated to the ordering along the chain direction. While the meso-peak2 for the HOMO polymer starts to decrease in intensity at $T$ > 60 °C, the meso-peak2 intensity for the RACO starts to drop immediately upon heating above ambient temperature. The intensity drop of the meso-peak2 is associated to a reduction in the long-range order along the direction of the helical chains. This seems to take place considerably before the onset of the phase transition (from WAXS) and the onset of chain elongation process (from Raman spectroscopy), especially for the RACO polymer, meaning that a rearrangement process along the chain axis (*i.e.*, rotation and chain unwinding to change handedness) and anticipating chain slipping and chain elongation (in the HOMO polymer) is thermally activated in the solid state inside the constricted mesophase globules. Moreover, Figure 8b shows that upon heating the meso-peak1 reflection shifts toward lower $q$-values, which means higher interchain spacings, for both grades. In agreement with the Raman results, the RACO polymer is characterized by an average larger interchain distance along the whole investigated temperature range.

Considering the above discussed results, we can conclude that the presence of the ethylene comonomers hinders an efficient chain interlock process, forcing the semi-ordered chains inside the mesomorphic domains to stay more separated throughout the entire meso-to-$\alpha$ transformation. Therefore, the chain extension process is suppressed as well in the RACO polymer. Nonetheless, the transition toward the $\alpha$-monoclinic structure takes place in the RACO regardless of a significant reduction (if not the absence) of efficient chain interlock and chain extension.

## 5. CONCLUSIONS

Here, we have conducted an *in situ* simultaneous SAXS/WAXS/Raman study on the thermal transitions occurring during heating of an iPP homopolymer and a propylene−ethylene random copolymer (with an ethylene content of 2.2%) processed in their mesomorphic phase. The acquired data have been analyzed using state-of-the-art (multiple) peak analysis to obtain the detailed trends in the change of peak area and peak position upon heating. The two investigated samples present mainly the transition from the initially defective mesomorphic to the ordered monoclinic $\alpha$ phase up to the onset of the melting process. Quantitative analysis of the Raman spectra provides clear information about the chain elongation and the chain interlock processes. The information extracted by Raman analysis was used to strengthen and complement the analysis of the mesomorphic WAXS reflections, providing information on structural changes occurring in the direction perpendicular and along the chain axis during the meso-to-$\alpha$ transition. Crystallite size evolution is instead tracked by SAXS.

Important details about the mechanism of the meso-to-$\alpha$ transition without and in the presence of ethylene comonomeric units are derived here, thanks to the complementarity of the X-ray and Raman information. The summary of the results discussed here shows how for the iPP homopolymer the meso-to-$\alpha$ transition is first characterized by an efficient chain interlock process accompanied by rotation and chain slipping in the temperature range 25−60 °C. Lateral chain displacement is still limited in this first stage of heating, while it is mainly occurring for $T$ > 60 °C. For $T$ > 80°, extensive helical chain elongation sets in, with shorted helical chain segments converting into helical segments of at least 12 and 14 units and longer. At $T$ ∼120 °C, the melting process starts where some of the crystallites melt and the most stable thickens before completely melting, as observed by SAXS analysis. The introduction of ethylene comonomers dramatically alters the transition mechanism. In the presence of ethylene units, rotation and chain slipping can still occur in the first stage of heating. On the contrary, the efficient chain interlock mechanism and the subsequent chain elongation occurring in


https://doi.org/10.1021/acs.macromol.1c01904
Macromolecules 2021, 54, 9681−9691

the iPP homopolymer are almost suppressed in the random copolymer. Nevertheless, the meso-to-$\alpha$ transition still occurs, but with the $\alpha$ crystallites in the random copolymer incorporating more structural defects and the ethylene comonomers, resulting in increased lateral interchain distance and larger crystallite dimensions with respect to the iPP homopolymer.

Our results demonstrate that the conformational pathways explored by the polymeric chains during the meso-to-$\alpha$ transition may be well different depending on the chemical nature of the iPP-based macromolecules. These differences are impossible to be tracked using only structural techniques such as X-ray diffraction. Our work suggests that quantitative analysis of high-quality *in situ* simultaneous SAXS/WAXS/Raman measurements can help in the future the scientific community to solve different problems related, but not limited, to polymer crystallization.

## ■ ASSOCIATED CONTENT

### Supporting Information

The Supporting Information is available free of charge at https://pubs.acs.org/doi/10.1021/acs.macromol.1c01904.

Example of the deconvoluted pattern for sample B9797 (HOMO) taken at a temperature of 130 °C, red hollow points corresponding to the fitted scattering profile, and WAXS crystallinity, calculated as sum of $\alpha$-phase + mesomorphic phase *versus* temperature for both the iPP grades (PDF)

## ■ AUTHOR INFORMATION


### Corresponding Authors

**Daniel Hermida-Merino** − *Netherlands Organisation for Scientific Research (NWO), DUBBLE@ESRF BP CS40220, Grenoble 38043, France; LMOPS, EA 4423, Université de Lorraine, CentraleSupelec Metz, Metz 57070, France*; Email: daniel.hermida_merino@esrf.fr

**Giuseppe Portale** − *Physical Chemistry of Polymeric and Nanostructured Materials, Zernike Institute for Advanced Materials, University of Groningen, Groningen 9747AG, The Netherlands; Dutch Polymer Institute, Eindhoven 5600 AX, The Netherlands;* orcid.org/0000-0002-4903-3159; Email: g.portale@rug.nl

### Authors

**Federico Di Sacco** − *Physical Chemistry of Polymeric and Nanostructured Materials, Zernike Institute for Advanced Materials, University of Groningen, Groningen 9747AG, The Netherlands; Dutch Polymer Institute, Eindhoven 5600 AX, The Netherlands;* orcid.org/0000-0002-8700-6151

**Sarah Saidi** − *Netherlands Organisation for Scientific Research (NWO), DUBBLE@ESRF BP CS40220, Grenoble 38043, France; LMOPS, EA 4423, Université de Lorraine, CentraleSupelec Metz, Metz 57070, France*

Complete contact information is available at: https://pubs.acs.org/10.1021/acs.macromol.1c01904



### Funding

This research was funded by the Dutch Polymer Institute, grant no. 810.

### Notes

The authors declare no competing financial interest.


## ■ ACKNOWLEDGMENTS

The ESRF and NWO are acknowledged for providing the beamtime at the BM26-DUBBLE beamline. The DUBBLE staff is acknowledged for the great support during the setup development and the beamtime. Borealis is acknowledged for providing the samples. Patrice Bourson is acknowledged for the help and discussions about the Raman results.

## ■ REFERENCES


(1) Natta, G.; Corradini, P. Structure and properties of isotactic polypropylene. *Il Nuovo Cimento* **1960**, *15*, 40−51.

(2) Gahleitner, M.; Paulik, C. Polypropylene and Other Polyolefins. *Brydson's Plastics Materials*, 8th ed.; Elsevier Ltd; 2017, pp 279−309.

(3) Lotz, B.; Wittmann, J. C.; Lovinger, A. J. Structure and morphology of poly(propylenes): A molecular analysis. *Polymer* **1996**, *37*, 4979−4992.

(4) Lotz, B. A new $\varepsilon$ crystal modification found in stereodefective isotactic polypropylene samples. *Macromolecules* **2014**, *47*, 7612−7624.

(5) Mileva, D.; Androsch, R.; Zhuravlev, E.; Schick, C.; Wunderlich, B. Formation and reorganization of the mesophase of isotactic polypropylene. *Mol. Cryst. Liq. Cryst.* **2012**, *556*, 74−83.

(6) Androsch, R.; Di Lorenzo, M. L.; Schick, C.; Wunderlich, B. Mesophases in polyethylene, polypropylene, and poly(1-butene). *Polymer* **2010**, *51*, 4639−4662.

(7) Corradini, P.; Petraccone, V.; De Rosa, C.; Guerra, G. On the Structure of the Quenched Mesomorphic Phase of Isotactic Polypropylene. *Macromolecules* **1986**, *19*, 2699−2703.

(8) Androsch, R. In situ atomic force microscopy of the mesomorphic-monoclinic phase transition in isotactic polypropylene. *Macromolecules* **2008**, *41*, 533−535.

(9) Cavallo, D.; Gardella, L.; Alfonso, G. C.; Mileva, D.; Androsch, R. Effect of comonomer partitioning on the kinetics of mesophase formation in random copolymers of propene and higher $\alpha$-olefins. *Polymer* **2012**, *53*, 4429−4437.

(10) Zia, Q.; Androsch, R.; Radusch, H.-J.; Piccarolo, S. Morphology, reorganization and stability of mesomorphic nanocrystals in isotactic polypropylene. *Polymer* **2006**, *47*, 8163−8172.

(11) De Rosa, C.; Auriemma, F.; Di Girolamo, R.; De Ballesteros, O. R. Crystallization of the mesomorphic form and control of the molecular structure for tailoring the mechanical properties of isotactic polypropylene. *J. Polym. Sci., Part B: Polym. Phys.* **2014**, *52*, 677−699.

(12) Mileva, D.; Androsch, R.; Zhuravlev, E.; Schick, C. Temperature of melting of the mesophase of isotactic polypropylene. *Macromolecules* **2009**, *42*, 7275−7278.

(13) van der Meer, D. W.; Varga, J.; Vancso, G. J. The influence of chain defects on the crystallisation behaviour of isotactic polypropylene. *Express Polym. Lett.* **2015**, *9*, 233−254.

(14) Gahleitner, M.; Bachner, C.; Ratajski, E.; Rohaczek, G.; Neißl, W. Effects of the catalyst system on the crystallization of polypropylene*. *J. Appl. Polym. Sci.* **1999**, *73*, 2507−2515.

(15) Gahleitner, M.; Jääskeläinen, P.; Ratajski, E.; et al. Propylene-ethylene random copolymers: Comonomer effects on crystallinity and application properties. *J. Appl. Polym. Sci.* **2005**, *95*, 1073−1081.

(16) Cavallo, D.; Portale, G.; Balzano, L.; et al. Real-time WAXD detection of mesophase development during quenching of propene/ethylene copolymers. *Macromolecules* **2010**, *43*, 10208−10212.

(17) Di Sacco, F.; Gahleitner, M.; Wang, J.; Portale, G. Systematic investigation on the structure-property relationship in isotactic polypropylene films processed via cast film extrusion. *Polymers* **2020**, *12*, 1636.

(18) Wallner, G. M.; Resch, K.; Teichert, C.; Gahleitner, M.; Binder, W. Effect of material structure and additives on the optical properties of PP cast films. *Monatsh. Chem.* **2006**, *137*, 887−897.

(19) Resch, K.; Wallner, G. M.; Teichert, C.; Gahleitner, M. Highly transparent polypropylene cast films: Relationships between optical properties, additives, and surface structure. *Polym. Eng. Sci.* **2007**, *47*, 1021−1032.

(20) Portale, G.; Troisi, E. M.; Peters, G. W. M.; Bras, W. Real-time fast structuring of polymers using synchrotron WAXD/SAXS techniques. *Polymer Crystallization II, Advances in Polymer Science*; Springer, 2017; Vol. *277*, pp 127−165.
(21) Wang, Z.-G.; Hsiao, B. S.; Srinivas, S.; et al. Phase transformation in quenched mesomorphic isotactic polypropylene. *Polymer* **2001**, *42*, 7561−7566.
(22) Thomann, R.; Wang, C.; Kressler, J.; Mülhaupt, R. On the γ-phase of isotactic polypropylene. *Macromolecules* **1996**, *29*, 8425−8434.
(23) Ponçot, M.; Martin, J.; Chaudemanche, S.; et al. Complementarities of high energy WAXS and Raman spectroscopy measurements to study the crystalline phase orientation in polypropylene blends during tensile test. *Polymer* **2015**, *80*, 27−37.
(24) Ma, Z.; Fernandez-Ballester, L.; Cavallo, D.; Gough, T.; Peters, G. W. M. High-stress shear-induced crystallization in isotactic polypropylene and propylene/ethylene random copolymers. *Macromolecules* **2013**, *46*, 2671−2680.
(25) Baeten, D.; Cavallo, D.; Portale, G.; Androsch, R.; Mathot, V.; Goderis, B. Combining fast scanning chip calorimetry with structural and morphological characterization techniques. *Fast Scanning Calorimetry*; Springer, 2016; pp 327−359.
(26) Nielsen, A. S.; Batchelder, D. N.; Pyrz, R. Estimation of crystallinity of isotactic polypropylene using Raman spectroscopy. *Polymer* **2002**, *43*, 2671−2676.
(27) Zhu, X.; Yan, D.; Yao, H.; Zhu, P. In situ FTIR spectroscopic study of the regularity bands and partial-order melts of isotactic poly(propylene). *Macromol. Rapid Commun.* **2000**, *21*, 354−357.
(28) Zhu, X.; Yan, D.; Fang, Y. In situ FTIR spectroscopic study of the conformational change of isotactic polypropylene during the crystallization process. *J. Phys. Chem. B* **2001**, *105*, 12461−12463.
(29) Hiejima, Y.; Takeda, K.; Nitta, K.-h. Investigation of the Molecular Mechanisms of Melting and Crystallization of Isotactic Polypropylene by in Situ Raman Spectroscopy. *Macromolecules* **2017**, *50*, 5867−5876.
(30) Portale, G.; Cavallo, D.; Alfonso, G. C.; et al. Polymer crystallization studies under processing-relevant conditions at the SAXS/WAXS DUBBLE beamline at the ESRF. *J. Appl. Crystallogr.* **2013**, *46*, 1681−1689.
(31) Saidi, S. *Multi-length Scale Study of the Impact of Fluoroelastomer Addition on the PVDF Structure by Coupled In Situ Measurements*; Université de Lorraine, 2020.
(32) Dyadkin, V.; Pattison, P.; Dmitriev, V.; Chernyshov, D. A new multipurpose diffractometer PILATUS@SNBL. *J. Synchrotron Radiat.* **2016**, *23*, 825−829.
(33) Li, X.; Ding, J.; Liu, Y.; Tian, X. A new model for mesomorphic-monoclinic phase transition of isotactic polypropylene. *Polymer* **2017**, *108*, 242−250.
(34) Strobl, G. R.; Schneider, M. Direct evaluation of the electron density correlation function of partially crystalline polymers. *J. Polym. Sci., Part A-2* **1980**, *18*, 1343−1359.
(35) Nikolaeva, G. Y.; Sagitova, E. A.; Prokhorov, K. A.; et al. Using Raman spectroscopy to determine the structure of copolymers and polymer blends. *J. Phys. Conf.* **2017**, *826*, 012002.
(36) Mileva, D.; Androsch, R.; Funari, S. S.; Wunderlich, B. X-ray study of crystallization of random copolymers of propylene and 1-butene via a mesophase. *Polymer* **2010**, *51*, 5212−5220.
(37) Zia, Q.; Mileva, D.; Androsch, R. Rigid amorphous fraction in isotactic polypropylene. *Macromolecules* **2008**, *41*, 8095−8102.
(38) Xu, M.; Liu, J. J.; Zhang, S.; et al. Influences of processing on the phase transition and crystallization of polypropylene cast films. *J. Appl. Polym. Sci.* **2014**, *131*, 41100.
(39) Mileva, D.; Androsch, R.; Cavallo, D.; Alfonso, G. C. Structure formation of random isotactic copolymers of propylene and 1-hexene or 1-octene at rapid cooling. *Eur. Polym. J.* **2012**, *48*, 1082−1092.
(40) Marega, C.; Causin, V.; Marigo, A. A SAXS-WAXD study on the mesomorphic-α transition of isotactic polypropylene. *J. Appl. Polym. Sci.* **2008**, *109*, 32−37.
(41) O'Kane, W. J.; Young, R. J.; Ryan, A. J. Simultaneous SAXS/WAXS and d.s.c. analysis of the melting and recrystallization behaviour of quenched polypropylene. *Polymer* **1994**, *35*, 1352−1358.
(42) Khafagy, R. M. In situ FT-Raman spectroscopic study of the conformational changes occurring in isotactic polypropylene during its melting and crystallization processes. *J. Polym. Sci., Part B: Polym. Phys.* **2006**, *44*, 2173−2182.
(43) Kobayashi, M.; Akita, K.; Tadokoro, H. Infrared spectra and regular sequence lengths in isotactic polymer chains. *Makromol. Chem.* **1968**, *118*, 324−342.
(44) Ruiz-Orta, C.; Fernandez-Blazquez, J. P.; Pereira, E. J.; Alamo, R. G. Time-resolved FTIR spectroscopic study of the evolution of helical structure during isothermal crystallization of propylene 1-hexene copolymers. Identification of regularity bands associated with the trigonal polymorph. *Polymer* **2011**, *52*, 2856−2868.
(45) Mileva, D.; Androsch, R.; Zhuravlev, E.; Schick, C. Critical rate of cooling for suppression of crystallization in random copolymers of propylene with ethylene and 1-butene. *Thermochim. Acta* **2009**, *492*, 67−72.
(46) Mileva, D.; Androsch, R. Effect of co-unit type in random propylene copolymers on the kinetics of mesophase formation and crystallization. *Colloid Polym. Sci.* **2012**, *290*, 465−471.
(47) Hosoda, S.; Hori, H.; Yada, K.-i.; Nakahara, S.-y.; Tsuji, M. Degree of comonomer inclusion into lamella crystal for propylene/olefin copolymers. *Polymer* **2002**, *43*, 7451−7460.
(48) Zhao, J.; Peng, Z.; Zhang, J.; Li, G. In situ FT-IR spectroscopy study on the conformational changes of quenched isotactic polypropylene during stepwise heating. *Polym. Bull.* **2011**, *67*, 1649−1659.
(49) Geng, Y.; Wang, G.; Cong, Y.; Bai, L.; Li, L.; Yang, C. Shear-induced nucleation and growth of long helices in supercooled isotactic polypropylene. *Macromolecules* **2009**, *42*, 4751−4757.
(50) Konishi, T.; Nishida, K.; Kanaya, T.; Kaji, K. Effect of isotacticity on formation of mesomorphic phase of isotactic polypropylene. *Macromolecules* **2005**, *38*, 8749−8754.
(51) McAllister, P. B.; Carter, T. J.; Hinde, R. M. Structure of the Quenched Form of Polypropylene. *J. Polym. Sci., Polym. Phys. Ed.* **1978**, *16*, 49−57.


https://doi.org/10.1021/acs.macromol.1c01904
*Macromolecules* 2021, 54, 9681−9691